Complementarities of high energy WAXS and Raman spectroscopy measurements to study the crystalline phase orientation in polypropylene blends during tensile test

Marc Ponçot, Julien Martin, Samuel Chaudemanche, Olivier Ferry, Thomas Schenk, Jean-Philippe Tinnes, David Chapron, Isabelle Royaud, Abdesselam Dahoun, Patrice Bourson

Accepted Manuscript

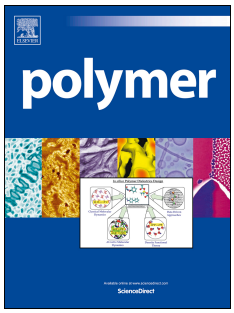

Complementarities of high energy WAXS and Raman spectroscopy measurements to study the crystalline phase orientation in polypropylene blends during tensile test

M. Ponçot, J. Martin, S. Chaudemanche, O. Ferry, T. Schenk, J.P. Tinnes, D. Chapron, I. Royaud, A. Dahoun, P. Bourson

PII: S0032-3861(15)30326-8

DOI: 10.1016/j.polymer.2015.10.040

Reference: JPOL 18207

To appear in: *Polymer*

Received Date: 13 July 2015

Revised Date: 7 September 2015

Accepted Date: 20 October 2015

Please cite this article as: Ponçot M, Martin J, Chaudemanche S, Ferry O, Schenk T, Tinnes JP, Chapron D, Royaud I, Dahoun A, Bourson P, Complementarities of high energy WAXS and Raman spectroscopy measurements to study the crystalline phase orientation in polypropylene blends during tensile test, *Polymer* (2015), doi: 10.1016/j.polymer.2015.10.040.

Graphical Abstract:

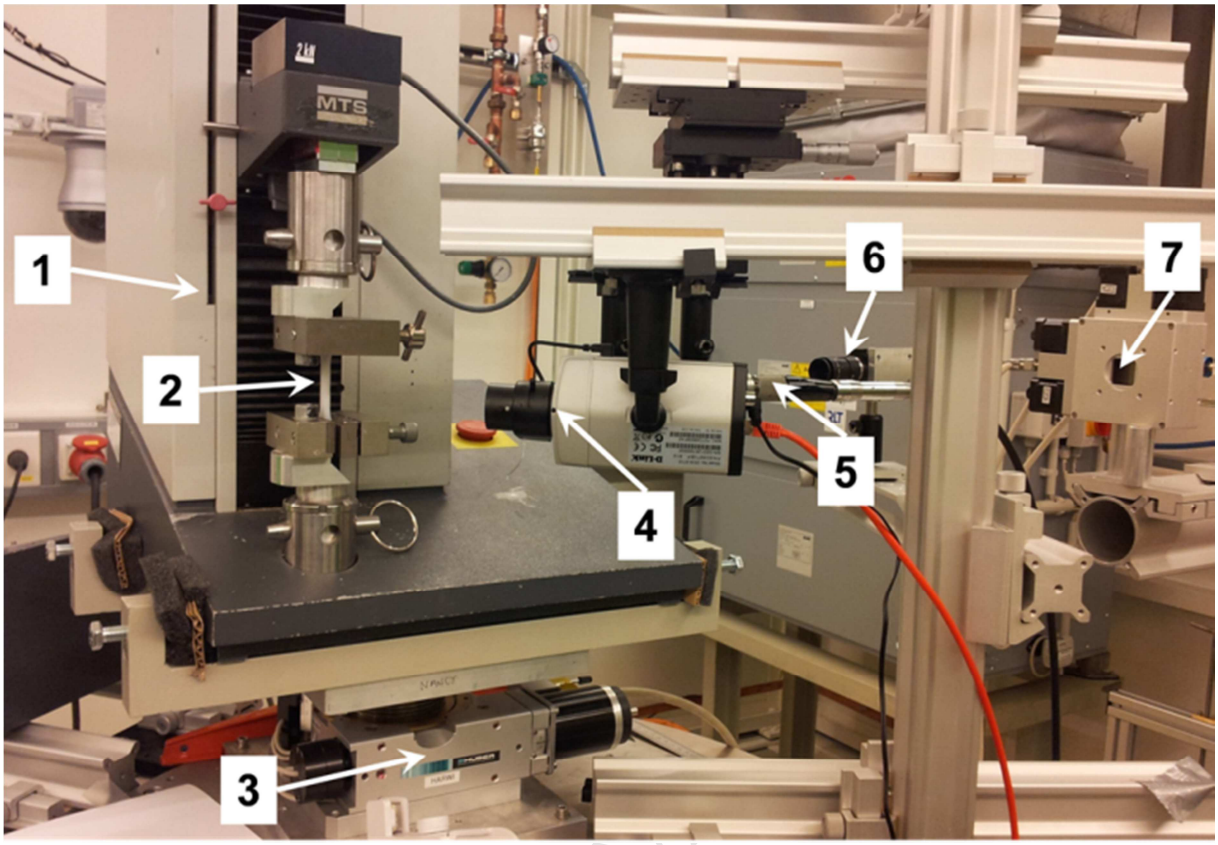

Special experimental set up developed to perform simultaneous high energy wide angle X-rays scattering (P07 beamline, PETRA III, DESY synchrotron, Hamburg, Deutschland) and Raman spectroscopy analysis during a mechanical tensile test: 1) Tensile test machine, 2) Dumbbell-shape specimen, 3) Z-motorized stage, 4) Video camera, 5) Raman head of probe, 6) VidéoTraction™ camera, 7) X-rays monochromator.

Complementarities of high energy WAXS and Raman spectroscopy measurements to study the crystalline phase orientation in polypropylene blends during tensile test

M. Ponçot[(1)*], J. Martin[(1)], S. Chaudemanche[(1)], O. Ferry[(1)], T. Schenk[(1)], J.P. Tinnes[(1)], D. Chapron[(2)], I. Royaud[(1)], A. Dahoun[(1)], P. Bourson[(2)]

(1) Institut Jean Lamour, UMR 7198 CNRS-Université de Lorraine,
Parc de Saurupt, CS 50840, 54011 Nancy Cedex, France
(2) LMOPS, Université de Lorraine, Supélec, EA 4423,
2 Rue E. Belin, F-57070 Metz, France

* Author to whom correspondence should be addressed

Abstract:

In situ measurements using simultaneously Raman spectroscopy and high energy wide angles X-rays scattering (HE-WAXS) were carried out during uniaxial tensile tests of different polypropylene blends (neat isotactic polypropylene – iPP, high impact polypropylene – iPP/EPR, and high impact polypropylene filled by 7%wt of µ-talc particles – iPP/EPR + µ-talc) at various strain rates (5.10^{-3} s^{-1}, 10^{-3} s^{-1} and 5.10^{-4} s^{-1}). Tensile tests were performed using the VidéoTraction™ system to determine the true mechanical behavior of materials in a Representative Volume Element (RVE) where microstructural analyses by the both experimental techniques are obtained. Evolutions of the macromolecular chains orientation have been obtained live at the macromolecular and crystalline cell scales. Experimental results show both that over the course of adding charges in the iPP matrix or increasing the true strain rate, this major micromechanism of deformation of semi-crystalline polymers would be less and less important until its complete disappearance in case of iPP/EPR filled by µ-talc particles. Moreover, correlations made between both techniques evidence similar results over a wide range of true strains. However, measurements diverge at lower and higher strains due to singularities of each both techniques which are discussed in terms of experimental protocols and materials microstructure modifications (transient mesophase, volume damage). Finally, the determination of the true intrinsic mechanical behaviors show similar stress hardening slopes for the three studied iPP blends which means that they all present an highly fibrillar microstructure. The differences of macromolecular chains orientation levels between each material is then discussed in terms of analysis volume of both techniques which could be responsible of their lack of accuracy in case of filled polymers.

Keywords: *Isotactic polypropylene; Ethylene propylene rubber; µ-talc; Wide angle X-ray scattering; Raman spectroscopy; Uniaxial tensile test; Chains orientation; Transient mesophase; Volume damage.*

1. Introduction

Relationships between mechanical properties and microstructure of materials, especially for solid polymers, represent the major key to better understand, control and predict their final in-use behavior. Numerous experimental works have been devoted to characterize the microstructural deformation mechanisms of polymers involved in uniaxial tension and many elementary descriptive models have been already proposed and discussed by the past [Peterlin, 1971; Schultz, 1974; Haudin *et al.*, 1982; Friedriech and Kausch, 1983]. They depend on the initial microstructures of polymers which are mainly induced by the formulation and the conformation processes. As a result, mechanical behaviour presents significant differences if the polymer matrix is amorphous (Boyce and Arruda, 1990; Bartczak *et al.*, 1996; Steenbrink *et al.*, 1997; Ponçot *et al.*, 2013), semi-crystalline (Ward, 1971; Samuels, 1971; G'sell *et al.*, 1997; Amornsakchai *et al.*, 2000; Séguela, 2007; Ponçot *et al.*, 2013; Pawlak *et al.*, 2014; Chaudemanche *et al.*, 2014) or filled with mineral and/or rubber particles (Bucknall *et al.*, 1972; Pukansky *et al.*, 1994; Plummer *et al.*, 1996; van der Wal and Gaymans, 1999; Nitta *et al.*, 2008; Mae *et al.*, 2008; Ponçot, 2009; Chaudemanche *et al.*, 2014). Chain orientation, shear banding, and volume damage (voids resulting from crazing or nodules/particles decohesion) are the main involved deformation micromechanisms whatever the initial microstructure of the considered material. The prevalence of one mechanism regarding the others induces such kind of mechanical properties differences. To investigate such mechanism of deformation of polymer blends involved during stretching, the need of fast and non-destructive techniques combining commodity in use is growing among the researchers community (Martin *et al.*, 2011, 2013; Ponçot *et al.*, 2012; Chaudemanche *et al.*, 2013). In this paper, two of them are performed simultaneously during uniaxial tensile tests to study the micromechanisms of deformation of different polypropylene blends (neat isotactic polypropylene, high impact polypropylene, and high impact polypropylene filled by 7%wt of µ-talc particles). They are high energy wide angle X-rays scattering – HE-WAXS (P07 beamline, PETRA III, DESY synchrotron, Hamburg, Deutschland) and Raman spectroscopy. HE-WAXS is a very suitable experimental technique to characterize the crystalline structure of semi-crystalline polymers. In case of neat polypropylene and its blends, crystallinity changes, phase transitions, crystalline macromolecular chains orientation, development of smectic mesophases during uniaxial tensile tests have been already explored (Davies *et al.*, 2010; Bao *et al.*, 2012). Although this method is really sensitive, it is not so simple to perform such experiments since the use of specific beamline at a synchrotron is needed. This paper

aims to compare results obtained by HE-WAXS with an experimental technique easier to perform at the laboratory scale or at the industry. Raman spectroscopy is well-suitable to determine the vibrational frequencies of the covalent chemical bonds of polymers and allow analysis of molecular species at different scales, from the chemical repetitive unit to the conformational architecture of the macromolecular chain (Koenig, 1999). The Raman spectra of isotactic polypropylene have been the object of several investigations and the assignment of Raman scattering bands are rather well established (Tadokoro et al., 1965; Fraser et al., 1973; Chalmers et al., 1991). Martin et al. (2011, 2013) have defined a specific spectral criterion which enables to characterize the macromolecular chains orientation of the crystalline phase of a neat iPP using a combination of different polarization geometries for both the incident and scattered radiations (Purvis and Bower, 1976; Cambon et al., 1987; Tanaka et al., 2006).

2. Experimental part

2.1. Materials

Isotactic polypropylene (iPP)

The semi-crystalline isotactic polypropylene that was investigated in this work was provided by Arkema (ref. 3050 MN1). The average molecular weights are $\overline{M}_n$ = 75,900 g.mol^{-1} and $\overline{M}_w$ = 262,000 g.mol^{-1} (Ponçot, 2009). The density determined by hydrostatic weighting is ρ = 0.946 g.cm^{-3}. The crystallinity index is X_c = 50 %vol. The glass transition temperature T_g (determined by dynamic mechanical analysis) and the melting temperature T_m (determined by differential scanning calorimetry) are 10°C and 167°C, respectively. Wide angle X-rays scattering analyses revealed the exclusive presence of the α-monoclinic crystal of iPP. The cell parameters are *a* = 6.666 Å, *b* = 20.78 Å, *c* = 6.495 Å, α = 90°, β = 99.6° and γ = 90° [Natta and Corradini (1960) ; Turner-Jones *et al.* (1994)]. Forming of the material is made by injection-molding of 4 mm thick plates.

Isotactic polypropylene/ethylene-propylene rubber (iPP/EPR)

The second polymer investigated is an isotactic polypropylene / ethylene-propylene rubber (iPP/EPR) supplied by Total Petrochemicals (ref. PPC 3650). The EPR content is 17 %wt. The final blend presents the following average molecular weights: $\overline{M}_n$ = 69,000 g.mol^{-1} and $\overline{M}_w$ = 599,000 g.mol^{-1}. As previously evidenced with scanning electron microscopy and transmission electron microscopy analysis, EPR nodules are homogeneously dispersed in the iPP matrix. They consist in “core-shell”-like particles of about 10 µm in diameter enclosing crystalline polyethylene lamellae (as revealed by transmission electron microscopy using ruthenium oxide coloration (Ponçot, 2009)). Then, differential scanning calorimetry analysis, performed at the standard heating rate of 10 °C.min^{-1}, reveals two melting peaks; a first one at 115 °C with a very low enthalpy (inferior to 1 J/g) which corresponds to the melting of polyethylene crystals contained in the EPR nodules (Ponçot, 2009) and a second one at 167 °C attributed to the melting of the α-iPP crystalline phase. The glass transition of the iPP matrix is still close to 10 °C while the EPR elastomeric phase exhibits a glass transition at - 45 °C (as revealed by dynamic mechanical analysis). Further WAXS analyses established that the average crystallinity index of iPP matrix is 45 %vol. (Ponçot, 2009). The samples were processed by injection moulding into 4 mm-thick plates.

Isotactic polypropylene/ethylene-propylene rubber filled with mineral fillers (iPP/EPR + µ-Talc)

The iPP/EPR previously described has been then modified by the addition of 7 %wt. µ-talc platelets as mineral fillers. The aspect ratio of these particles is about 5.5 with an average length of 25µm and an average thickness of 5µm. Neither chemical nor mechanical treatments are applied to these particles before their mixing with the iPP/EPR matrix. Differential scanning calorimetry analysis reveals the two previously identified peaks at 115 °C and 164 °C attributed to the melting of the polyethylene crystals present in the EPR nodules and α-iPP crystals, respectively. The presence of a third small peak located at 146 °C, usually attributed to the melting of β-iPP crystals, inform us about the fact that µ-talc particles promotes their creation i) due to their nucleation effect (Lotz *et al.*, 1996) and ii) because they increase the blend viscosity (higher shear effect during the forming process by injection molding) as introduced by Kantz *et al.* in 1972. The average crystallinity index determined by DSC measurements and confirmed by WAXS experiments is about 55 %vol. which is 10 %vol. more than the one determined in the case of the iPP/EPR. Samples were processed by injection molding into 5 mm-thick plates.

2.2. Experimental setup

Mechanical testing equipment

The video-controlled mechanical testing method used in this paper is the VidéoTraction™ system (G'sell *et al.*, 1992; G'sell *et al.*, 2002; Addiego *et al.*, 2006; Ponçot, 2009, Ponçot *et al.*, 2013). For different deformation paths, it gives access to the true mechanical behaviour of polymers by taking into account of the development of the polymer necking. Video measurements are performed locally at the centre of the sample in a specific Representative Volume Element (RVE) where plastic deformation appears. To ensure the localization of the necking zone at the centre of the sample, width of the dumbbell-shaped specimen is slightly reduced by milling (reduction of 6 % of the specimen width). The axial true strain in the RVE, ε_{33}, is obtained by a polynomial interpolation of partial strains measured from the displacement of axial markers using Lagrange polynomial interpolation and following Hencky' strain theory. For uniaxial tensile testing, transverse strains in the RVE, ε_{11} and ε_{22}, are equal considering the realistic hypothesis that the strain field is transversally isotropic in the centre of the neck (Bucknall *et al.*, 1972; Naqui and Robinson, 1993; Pukansky *et al.*,

1994; G'sell *et al.*, 2002; Addiego *et al.*, 2006; Ponçot, 2009). Lastly, the volume strain in the RVE, ε_v, is computed as the trace of the true strain tensor:

$$\varepsilon_v = \varepsilon_{11} + \varepsilon_{22} + \varepsilon_{33} \quad (1)$$

The axial true stress (Cauchy stress) is determined in the same RVE as the load per unit actual cross-section:

$$\sigma_{33} = \frac{F}{S_0}\exp(-2\varepsilon_{11}), \quad (2)$$

where S_0 is the initial cross-section of the tensile specimen.

All the mechanical tests were performed at room temperature (22 °C). It is also worth noting that VidéoTraction™ system enables to perform tensile testing at constant axial true strain rate. The influence of the true axial strain rate on both the mechanical behaviour and deformation mechanisms of iPP and modified iPP was also investigated. Various true strain rates (5.10^{-3} s^{-1}, 10^{-3} s^{-1} and 5.10^{-4} s^{-1}) were chosen in such a way to ensure the control loop of the testing machine actuator and to avoid any self-heating of the material during the mechanical testing [Billon, 2003; Ye, 2015].

Raman spectroscopy analysis

Raman scattering experiments were performed using a RXN1 Kaiser micro-spectrometer linked to a remote head of probe by means of two optical fibers. A 300 mW laser diode emitting a 785 nm exciting line was used which allows reducing fluorescence emission and local heating of the polymer specimen. All spectra were recorded in backscattered geometry with a working distance of 20 cm. Within such configuration, the laser waist on the specimen is about 0.16 mm^3. The micro-spectrometer is equipped with a 1200 $gr.mm^{-1}$ grating and a spectral resolution of about 1 cm^{-1} is achieved. Rayleigh scattered light is eliminated through a holographic Notch filter. Before each tensile test, shift in the Raman spectra is calibrated with the silicon band located at 521 cm^{-1}. An individual spectrum recording lasts a few seconds depending on the resolution and the true strain rate at the time of *in situ* analysis during stretching.

The crystalline macromolecular chains orientation is estimated from Raman spectra by performing acquisitions in particular polarization geometry of the incident and scattered radiations where both the incident and scattered radiations are polarized along the stretching direction I. Following these conditions, we demonstrated in previous papers that the ratio $I_{973cm\text{-}1}$ / $I_{998cm\text{-}1}$ of the integrated intensity of the two particular Raman scattering bands at 973 cm^{-1} (symmetric stretching mode of the C-C skeletal backbones in crystalline phase) and

998 cm^{-1} (rocking mode of CH_3 lateral alkyl groups in crystalline phase), enable to estimate orientation of crystalline phase chains in the tensile direction I (Ponçot, 2009; Martin, 2009; Martin *et al.*, 2011, 2013; Ponçot *et al.*, 2011, 2012; Chaudemanche, 2011; Chaudemanche *et al.*, 2013).

Synchrotron 2D WAXS measurements

Experiments were carried out in the PETRA III synchrotron facility at the DESY laboratory (Hamburg – Germany) on the P07 – High Energy Materials Science beamline. The beam energy was about 60 keV (λ = 0.0206 nm). The beam cross section was 150 x 150 µm². The samples were analyzed using Wide Angle X-ray Scattering (WAXS) in transmission. The scattered beam was collected with a PerkinElmer XRD1622AP digital flat panel detector. The chosen high energy resulted in a low X-ray absorption in the polymer (6.8% for a 4 mm thick sample). Coupled with the relatively short duration of the tensile tests, this leads to no measurable heating of the polymer or radiation degradation, despite the beam's high influence, characteristic of synchrotrons radiations. A one second frame was acquired every second for samples tested at a true strain rate of 10^{-4} s^{-1}, whereas for samples tested at a 10^{-3} s^{-1}, the acquisition time was of a 0.5 second frame every 0.5 second. The distance between the detector and the sample was about 1.36 m, allowing us to focus on low scattering angle. Thus, both the central scattering zone corresponding to amorphous material and the diffractions patterns of the crystalized polymer and mineral charges were recorded with a good precision. With our detector, at the wavelength used for the experiment, measurements were realized with a 2-θ step of 0.0084°, up to a value of 12° (corresponding to Q-vector space values of a 0.044 nm^{-1} step, up to 62 nm^{-1}). The WAXS patterns were integrated with Fit2D to produce 1-dimensional intensity-vs-2theta graphs. The stretching direction (I) is always vertical on the acquired 2D WAXS patterns.

The orientation level of the crystallites can be formalized on a quantitative numerical basis using Hermans' orientation function $F_{\vec{X}/I}$ which describes the orientation of a given crystallographic axis $\vec{X}$ relative to one reference direction, usually the stretching direction (I). Its general expression is:

$$F_{\vec{X}/I} = \frac{3 < \cos^2\left(\alpha_{\vec{X}/I}\right) > -1}{2} \qquad (3) \quad \text{with:} \quad < \cos^2\left(\alpha_{\vec{X}/I}\right) >= \frac{\int_0^{\pi/2} I_{hkl} \cdot \cos^2\varphi \cdot \sin\varphi \cdot d\varphi}{\int_0^{\pi/2} I_{hkl} \cdot \sin\varphi \cdot d\varphi} \qquad (4)$$

where I_{hkl} represents the maximal intensity scattered by the (*hkl*) planes relative to a given crystallographic axis $\vec{X}$ as a function of the azimuthal angle φ (Hermans and Weidinger, 1948).

Table 1 develops the meaning of the Hermans' orientation factor values related to the specific crystallographic orientation.

$<\cos^2(\alpha_{\vec{X}/I})>$	$F_{\vec{X}/I}$	Texture
0	- 1/2	I is perpendicular to $\vec{X}$
1/3	0	Isotropic distribution of I in space
1/2	1/4	Isotropic distribution of I in the plane parallel to $\vec{X}$
1	1	I is parallel to $\vec{X}$

Table 1: Remarkable values of $F_{\vec{X}/I}$ in relation to the associated crystalline macromolecular textures.

Synchrotron Wide Angles X-rays Scattering (WAXS), Raman spectroscopy and VidéoTraction™ coupling system

The experimental set-up in Figure 1 was specifically designed to characterize the polymer micro-structure at different scales in real time with the course of a uniaxial tensile test and is based on the system patented by Dahoun *et al.* in 2011. It consists in the combination of a video-controlled tensile test machine (1) using the VidéoTraction™ system (6) with a Raman spectrometer and a synchrotron High Energy WAXS beam line. They are fixed up on a 3-D directions movable hexapod. Before each tensile test, laser from the Raman head of probe (5) and X-rays beam from the X-ray monochromator (7) are strictly aligned towards the RVE of the polymer specimen (2) which is gripped between the clamps of the tensile-testing machine. Since uniaxial tension is applied by the displacement of the upper grip, gradual misalignment of the RVE with respect to laser and X-ray beams is expected. Thanks to a video camera continuously pointed to the polymer specimen and linked to a z-motorized stage (3) via a control loop, both the laser and X-ray beams remain aligned with the RVE during the entire course of the tensile test.

3. Experimental results

3.1 True mechanical behavior

Influence of the polymer formulation

Since glass transition temperatures of EPR (-45 °C) and iPP (10 °C) are below the room temperature, all the specimens that were uniaxially stretched in this work are in their rubber state. Figure 2 shows the tensile curves recorded at a constant true strain rate (5.10^{-3} s^{-1}) for the three considered polymers, iPP, iPP/EPR and iPP/EPR/µtalc. In Figure 2 a), despite the different values of stress and strain at the yield point (σ_y = 36,2 MPa and ε_y = 0,09 for iPP ; σ_y = 23,2 MPa and ε_y = 0,07 for iPP/EPR), it is to be noticed that the tensile curve of iPP presents a similar shape to that of iPP/EPR until the plastic plateau (which begins at ε_p = 0,27 and ε_p = 0,18 for iPP and iPP/EPR, respectively) including a weak softening stage for both. Young's moduli are calculated at the lowest values of strain at the early stage of the visco-elastic domain. They are equal to 1695 MPa and 1130 MPa for iPP and iPP/EPR, respectively. The influence on mechanical toughness of the addition of the viscoelastic EPR phase into the iPP matrix is there clearly put in evidence. Then, the extents of the plastic plateau are different one to the other: the strain-hardening occurs earlier in terms of true strain value in case of iPP/EPR and shows a more important increase of the slope of the stress/strain curves at the highest values of strain. The addition of 7 %wt. of µ-talc particles into the iPP/EPR polymer blend strongly modifies the true mechanical behavior as indicated in Figure 2 a). The Young's modulus is about 2025 MPa which is higher than the one determined for iPP. Moreover, the achieved stress level in comparison to the neat isotactic polypropylene is increased. Concerning yielding, it occurs at a stress value situated between the iPP and iPP/EPR. It is noticed that the yield strain is the lowest of all the studied materials which indicates that the plastic damage takes place earlier. Finally, the magnitude of the strain-hardening is similar to the one observed in case of iPP. Figure 2 b) illustrates the evolutions of the volume strain (calculated by the Equation 1) as a function of the axial true strain corresponding to the mechanical behaviors of Figure 2 a) for all the three materials. All curves show an almost linear evolution with stretching. Mainly the magnitudes are different. The addition of EPR nodules increases the volume strain in comparison to the neat matrix. This effect is emphasized by the introduction of mineral particles of µ-talc.

Influence of true strain rate

The influence of true strain rate in the range of 5.10^{-4} s^{-1} to 1.10^{-3} s^{-1} on the true mechanical behavior of polymers is presented in Figure 3. An increase of stress is observed up to moderate strain levels with increasing the stretching rate whatever the material. Then, the yield point is higher for neat iPP than for the blends whatever the studied strain rate. Different amplitudes of microstructural softening appear since organic and mineral charges promote microstructural damages to macromolecular rearrangements in the blends. Stronger softening is observed in case of iPP/EPR + µ-talc. Then, plasticity is characterized by a quite large plateau for all materials. Strain-hardening takes place at large strain level. However, during the strain-hardening stage, the stress–strain curves are not parallel anymore for the two filled materials, as indicated in Figure 3. This phenomenon does not enable to predict the tensile behavior at large strain level using phenomenological constitutive equations as the one proposed by G'sell and Jonas (1979) (Ponçot, 2009 ; Ponçot *et al.*, 2013).

3.2 2D WAXS patterns

Combination of the VidéoTraction™ system with WAXS acquisitions allows us to follow the evolution of the crystalline phase during the uniaxial true tensile test with high time resolution. Figure 4 shows three sets of 2D WAXS patterns recorded at different true strain level for the three different polymers investigated (T = 22 °C and $\varepsilon = 5.10^{-4}s^{-1}$). Patterns at null true strain value are indexed in terms of characteristic scattering crystallographic planes of the polypropylene monoclinic crystalline cell ((110), (040), (130), (111) and (131)). It can be noticed that the three materials show quasi-isotropic rings at the initial state for all values of the azimuthal angle (0° to 360°). Only weak variations of the intensity are observed for filled polypropylene (iPP/EPR and iPP/EPR filled with µ-talc) suggesting a slight orientation of the crystalline phase at the initial state. Additional rings are naturally present in 2D WAXS

Depending on the polymer formulations the rings intensity towards the azimuthal angle does not present the same evolution as a function of true strain. In case of neat iPP and iPP/EPR, most of the initial rings change into highly illuminated arcs as a result of stretching with a phenomena more pronounced for neat iPP. Concerning iPP/EPR filled with µ-talc, only weak modifications of the rings intensity distribution towards the azimuthal angle can be observed for high true strain values superior to 0.6 and they do not result in the appearance of arcs but in a kind of an equatorial diffusion. This diffraction peak tendency to collapse is widely more developed in case of iPP, followed by iPP/EPR and finally by iPP/EPR + µ-talc.

The macromolecular chains orientation of the iPP crystalline phase, as one of the main micromechanisms of deformation of uniaxially stretched semi-crystalline polymers, is focused. From 2D WAXS patterns, the Hermans'factor $F_{\vec{b}/I} = F_{(040)/I}$ is then calculated. Indeed, the normal direction of this particular crystallographic plane of the α monoclinic cell is strictly perpendicular to the $\vec{c}$ axis, the backbone chains direction. Figure 5 reports the variation of this Hermans' orientation factor as a function of the axial true strain for various true strain rates and for the three polymers that were investigated in this study.

Firstly, it has to be noticed that the three studied material show a weak initial texture induced by the forming process by injection molding ($F_{(040)/I} = -0.12$, $F_{(040)/I} = -0.1$ and $F_{(040)/I} = -0.06$ for iPP, iPP/EPR and iPP/EPR filled with µ-talc, respectively). Mechanical probes are then machined out in the manner that this crystalline orientation of the macromolecular chains is taken as the stretching direction. Addition of organic and mineral charges into the iPP matrix reduces the initial texture involved by the injection molding process. This is the reason why a small variation of $F_{(040)/I}$ towards 0 (isotropic microstructure) is observed at the earliest true axial strain values in cases of iPP and iPP/EPR until the middle of the respective plastic plateaus. It could be actually attributed to a first step of reorganization of the initial crystalline texture previous to the main effect of macromolecular chains orientation induced by stretching which is then responsible of the decrease of $F_{(040)/I}$. This effect is not observable for iPP/EPR + µ-talc and in case of iPP/EPR stretched at the lowest true strain rate (5.10^{-4} s^{-1}). Influence of this last mechanical test parameter is the most evident for neat iPP: higher is the true strain rate; lower is the crystalline chains orientation all along stretching. Secondly, over the course of adding charges in the iPP matrix, Hermans' orientation factors show that this major micromechanism of deformation of semi-crystalline polymers seems less and less important until its complete disappearance in case of iPP/EPR + µ-talc. Indeed, experimental results evidence that the magnitude of the crystalline chains orientation changes a lot depending on the material formulation. $F_{(040)/I}$ in case of the neat iPP reaches close values of -0.5 whatever the strain rate which is characteristic of a highly fibrillar microstructure along the stretching direction I. The addition of the EPR nodules reduces much this micromechanism. Maximal value of $F_{(040)/I}$ is around of -0.25. Finally, experimental results demonstrate that presence of µ-talc particles in the modified iPP/EPR polymer seems to inhibit almost totally the crystalline chains orientation of the iPP matrix.

3.3 Raman spectroscopy

Figure 6 presents the variations of the ratio $I_{973cm-1}$ / $I_{998cm-1}$ as a function of the true strain for the three studied materials and for at least two true strain rates. Apart from the initial disorientation phenomenon previously observed by WAXS, a similar description of the evolutions of the $I_{973cm-1}$ / $I_{998cm-1}$ ratio as for $F_{(040)/I}$ is available regarding the influences of the materials formulation and the true strain rate: orientation micromechanism seems to disappear adding organic and mineral fillers and in the same way the sensitivity towards the true strain rates decreases. Some differences between results of both techniques can be observed in case of iPP at the very low and high levels of true strain. The evolution of the Raman criterion keeps constant at the beginning of the stretching test whereas it was noticed a variation of the WAXS Hermans' factor. In the inverse manner, $I_{973cm-1}$ / $I_{998cm-1}$ still increases at high true strain values whereas $F_{(040)/I}$ reaches a plateau close to -0.5. For the three materials, the initial value of $I_{973cm-1}$ / $I_{998cm-1}$ is about 2. It means that the crystalline macromolecular chains present an initial orientation due to injection molding taking as the stretching direction. Martin *et al.* (2013) have already showed that in case of non-textured neat iPP, the initial value of the criterion is 1.5.

4. Discussion

Macromolecular chains orientation is a main micromechanism of deformation of polymers upon stretching. In this paper, it was measured *in situ* at the Desy beamline of PETRA III Synchrotron (Hamburg) simultaneously by WAXS and Raman spectroscopy for three different polymer blends. Both experimental techniques gave the quantification of the evolution of the crystalline chains orientation in real time during a uniaxial tensile test. As highlighted on Figure 7, they show good correlations one to the other whatever the studied iPP blend over a wide range of true strain.

Even if the two evolutions of the orientation factors determined by Raman spectroscopy and WAXS are similar on a wide range of deformation for all the studied polypropylene blends, singularities can be noticed at low and high true strain values especially for iPP and iPP/EPR.

i) Results diverge at lower strains due to the better sensitivity of the WAXS orientation factor to characterize the probe plane distribution of the crystalline macromolecules deduced from the intensity profile of crystallographic planes identified in the iPP monoclinic crystals (Figure 8 a)). In the opposite, Raman spectroscopy only gets vibrational signal from the iPP molecular bonds when they are oscillating in the same direction as the Raman laser polarization (Figure 8 b)). However, the valence angle value of the C-C bond (109°28') in the iPP carbon skeleton and the helical helix 3_1 of the macromolecule are sources of errors which could be responsible of the lack of accuracy of this technique since the laser is strictly polarized in the stretching direction. So Raman spectroscopy cannot be sensitive enough to detect the small magnitude of orientation. That is the reason why the residual melt flow orientation induced at the time of injection molding of the studied polymer plates is only detectable from 2D WAXS patterns.

At the early stages of deformation, the Hermans' orientation factor tends to zero. It denotes the prior macromolecular reorientation by the gliding lamellae and the tie molecules stretching. The addition of fillers and especially µ-talc particles is reducing the orientation induced by the conformation process and then this last effect too.

ii) Results move apart at the highest strain values due to the better accuracy of the Raman measurements despite the decrease of the analyzed volume of matter in the RVE during stretching. The orientation factor linearly increases until the end of the mechanical test. In the case of WAXS measurements, the Hermans' factor is affected by an important diffusive effect. Patterns reveal well the development of the so-called smectic mesophase (Natta *et al.*,

1959; Androsch *et al.*, 2010) which presents a similar crystalline structure to α's but with a lot of imperfections. This is the reason why the diffraction peaks of the WAXS patterns are enlarged as illustrated in Figure 9 for iPP and iPP/EPR. This diffusion phenomenon is responsible of the lack of X-rays scattering precision in addition to the over whole intensity decrease. The mesophase is weakly observable in case of iPP/EPR + µ-talc (Liu *et al.*, 2013) due to the predominance of the volume damage micromechanism of deformation in case of filled polypropylene matrixes. The macromolecules orientation keeps low or highly located in the polymer fibrils.

The three isotactic polypropylene blends exhibit singular true mechanical behaviors in uniaxial tension depending on the type of fillers as revealed by figures 2 and 3. The introduction of EPR nodules inside the iPP matrix reduces drastically the yield and plastic stresses in comparison to the neat polymer. Addition of µ-talc improves the viscoelastic resistance of the high impact polypropylene, whereas the plastic stress becomes and stays inferior to the neat matrix. Even the stress hardening stage is less pronounced for this last blend. It was observed in Figure 2 b) that volume strain increases with the amount and the diversity of the added fillers. The iPP/EPR + µ-talc blend shows the most predominant effect.

As described by Ponçot (2009) and Ponçot *et al.* (2013), volume strain was taken into account to determine the true intrinsic mechanical behaviors of polymer materials without voids. The true stress and the true strain are recalculated using the equations previously established in order to obtain the true intrinsic stress and the true intrinsic strain which represent the true intrinsic mechanical behavior of the solid polymer without cavities. The corrected mechanical curves are then presented in Figure 10. No significant change happens before the materials plasticity since volume strain keeps low. At the largest strain values, similar slopes of the stress hardening are observed between the three different polymer blends. Stress hardening is usually attributed to a highly fibrillar microstructure where macromolecules are wholly aligned along the stretching direction (I). Consequently, in both cases (iPP/EPR and iPP/EPR + µ-talc), the fibrils located between two adjacent voids should be made of highly oriented macromolecular chains of iPP.

Indeed, first step of plasticity in case of polymers filled with core-shell elastomer nodules is their own destruction upon stretching what results in the development of 45° oriented dilatational shear bands as presented in Figure 11 (Jang, 1985; Wu, 1985; Lazzeri and Bucknall, 1993; Dagli *et al.*, 1995; Zebarjad *et al.*, 2004; Nitta and Yamaguchi, 2008; Ponçot,

2009). As a result, the iPP fibrils located between two adjacent destroyed nodules should be then composed with highly oriented macromolecular chains along the stretching direction.

When iPP/EPR blends are filled with mineral particles, many authors have demonstrated that whatever the considered fillers and the cohesion level with the iPP matrix, the first micromechanism of deformation involved during stretching is cavitation due to the mineral particles decohesion with the polymer matrix (Pukanzky *et al.*, 1994; Mae *et al.*, 2008; Ponçot, 2009; Chaudemanche *et al.*, 2014). In the same way as previously discussed, the iPP fibrils located between two adjacent voids should be then composed with highly oriented macromolecular chains along the stretching direction.

However, both techniques show a weak orientation effect during stretching for iPP/EPR and iPP/EPR + µ-talc (Figures 5 and 6), whereas regarding the true intrinsic mechanical behaviors (relative to the iPP main matrix), similar stress hardening magnitude are observed for all three materials whatever their formulation. It can be discussed in terms of analysis volume of both techniques. In case of WAXS, the beam cross section was 150 µm x 150 µm = 0.022 mm². For Raman spectroscopy, the volume of the waist was 0.16 mm^3 which corresponds to a diameter of about 80 µm and a circular cross section of about 0.021 mm² (Chaudemanche, 2013). These two dimensions are largely bigger than the micro-fibrils and voids as revealed by scanning electron microscopy observations resumed in Figure 12. The volume fraction of highly oriented crystalline macromolecular chains is then really weak in comparison of those made of voids and undamaged iPP matrix. That is the reason why it cannot be detected by both used experimental techniques.

5. Conclusion

The coupling sytem of VidéoTraction™, WAXS and Raman spectroscopy especially designed to establish the narrow relationship between polymer blends microstructure evolution and mechanical behaviors and properties was used at the DESY laboratory of PETRA III synchrotron. The work focused on neat and filled iPP matrix. The modifications of the mechanical properties due to the gradual complexity of formulations (addition of EPR nodules and µ-talc particles) were explained in terms of influence of the micromechanisms of deformation during a uniaxial stretching at true strain rates. Good correlations are obtained between orientation factors determined by WAXS and Raman spectroscopy. Singularities were highlighted: WAXS is more efficient at lower strains to observe the prior reorientation of the crystalline chains, however at the time of plasticity the signal is interfered by the development of a crystalline mesophase; Raman spectroscopy is not sensitive to the reorientation phenomenon at low strain values due to the initial laser polarization in the stretching direction, however it enables to follow the orientation until the end of the mechanical test. The true intrinsic mechanical behaviors are then determined and give finally the real mechanical behavior of blends evicting the inside voids. Similar strain hardenings were obtained whatever the blend when the volume strain correction is applicate. However, macromolecular orientation levels are totally different. It was explained by the dimensions of the analysis volume of the used experimental techniques which are too large to locally measure the orientation gathered right in the micro-fibrils, “alone” matter between two adjacent voids. The more elevated is the volume strain; the lower is the measured macromolecular orientation whereas similar stress hardening slopes are obtained.

Acknowledgement:

The P07 – High Energy Materials Science beamline of PETRA III synchrotron facility at the DESY laboratory (Hamburg – Germany).

References:

Addiego F., Dahoun A., G’sell C., Hiver J.M., “*Characterization of volume strain at large deformation under uniaxial tension in high-density polyethylene*”, Polymer, 47, 4387-4399, (2006)

Androsch R., Di Lorenzo M.L., Schick C., Wunderlich B., “*Mesophases in polyethylene, polypropylene, and poly(1-butene)*”, Polymer, 51, 4639-4662, (2010)

Amornsakchai T., Olley R.H., Basset D.C., Al-Hussein M.O.M., Unwin A.P., Ward I.M., "*On the influence of initial morphology on the internal structure of highly drawn polyethylene*", Polymer, 41 (23), 8291-8298, (2000)

Bao R., Ding Z., Zhong G., Yang W., Xie B., Yang M., "*Deformation-induced morphology evolution during uniaxial stretching of isotactic polypropylene: effect of temperature*", Colloid and Polymer Science, 290 (3), 261-274, (2012)

Bartczak Z., Galeski A., Argon A.S., Cohen R.E., "*On the plastic deformation of the amorphous component in semicrystalline polymers*", Polymer, 37, 2113-2123, (1996)

Billon N., "*Thermal effects during mechanical characterisation of solid polymers*", Mécanique & Industries, 4, 357-364, (2003)

Boyce M.C., Arruda E.M., "*An experimental and analytical investigation of the large strain compressive and tensile response of glassy polymers*", Polymer Engineering and Science, 30, 1288-1298, (1990)

Bucknall C.B., Clayton D., "*Rubber-toughening of plastics, part 1: Creep mechanisms in HIPS*", Journal of Materials Science, 7, 202-210, (1972)

Cambon L.D., Ramonja J.L., Luu D.V., "*Raman-laser study of isotactic polypropylene-uniaxial drawing deformation*", Journal of Raman Spectroscopy, 18, 129-132, (1987)

Chalmers J.M., Edwards H.G.M., Lees J.S., Long D.A., Mackenzie M.W., Willis H.A., "*Raman spectra of polymorphs of isotactic polypropylene*", Journal of Raman Spectroscopy, 22 (11), 613-618, (1991)

Chaudemanche S., Ph.D. Thesis, Lorraine University-Jean Lamour Institute, Nancy, France (2013)

Chaudemanche S., Ponçot M., André S., Dahoun A., Bourson P., "*Evolution of the Raman backscattered intensity used to analyze the micromechanisms of deformation of various polypropylene blends in situ during an uniaxial tensile test*", Journal of Raman Spectroscopy, 45, 369–376, (2014)

Dagli G., Argon A.S., Chen R.E., "*Particle size effect in craze plasticity of high-impact polystyrene*", Polymer, 36 (11), 2173-2180, (1995)

Dahoun A., Bourson P., Martin J., Ponçot M., "*Dispositif de détermination du comportement mécanique local d'une éprouvette de matériau*", Patent FR 2981452 (B1) / WO 2013054062 (A1), Lorraine University (France), (2011)

Davies R.J., Zafeiropoulos N.E., Schneider K., Roth S.V., Burghammer M., Riekel C., Kotek J.C., Stamm M., "*The use of synchrotron X-ray scattering coupled with in situ mechanical testing for studying deformation and structural change in isotactic polypropylene*", Colloid and Polymer Science, 282 (8), 854-866, (2004)

Fraser G.V., Hendra P.J., Watson D.S., Gall M.J., Willis H.A., Cudby M.E.A, "*The vibrational spectrum of polypropylene*", Spectrochimica Acta Part A: Molecular Spectroscopy, 29 (7), 1525-1533, (1973)

Friedriech K., Kausch H.H., *Advances in Polymer Science, Crazing in Polymers*, 52/53, Springer-Verlag, Berlin-Heidelberg, (1983)

G'Sell C., Dahoun A., Favier V., Hiver J.M., Philippe M.J., Canova G.R., "*Microstructure transformation and stress-strain behavior of isotactic polypropylene under large plastic deformation*", Polymer Engineering and Science, 37 (10), 1702-1711, (1997)

G'sell C., Hiver J.M., Dahoun A., "*Experimental characterization of deformation damage in solid polymers under tension and its interrelation with necking*", International Journal of Solids and Structures, 39, 3857-3872, (2002)

G'sell C., Hiver J.M., Dahoun A., Souahi A., "*Video-controlled tensile testing of polymers and metals beyond the necking point*", Journal of Materials Science, 27, 5031-5039, (1992)

G'sell C., Jonas J.J., "*Determination of the plastic behaviour of solid polymers at constant true strain rate*", Journal of Materials Science, 14 (3), 583-591, (1979)

Haudin J.M., Escaig B., G'Sell C., *Plastic Deformation of Amorphous and Semi-Crystalline Materials*, Les Editions de Physique, Les Ullis, (1982)

Hermans P.H., Weidinger A., "*Quantitative X-ray investigations on the crystallinity of cellulose fibers. A background analysis*", Journal of Applied Physics, 19 (5), 491-506, (1948)

Jang B.Z., "*Rubber toughening in polypropylene*", Journal of Applied Polymer Science, 30

(6), 2485-2504, (1985)

Koenig J.L., *Spectroscopy of Polymers*, 2nd edition, Elsevier Science, New York, (1999)

Lazzeri A., Bucknall C.B., "*Dilatational bands in rubber-toughened polymers*", Journal of Materials Science, 28 (24), 1573-4803, (1993)

Liu P., White K.L., Sugiyama H., Xi J., Higuchi T., Hoshino T., Ishige R., Jinnai H., Takahara A., Sue H-J., "*Influence of Trace Amount of Well-Dispersed Carbon Nanotubes on Structural Development and Tensile Properties of Polypropylene*", Macromolecules, 46, 463-473, (2013)

Mae H., Omiya M., Kishimoto K., "*Microstructural observation and simulation of micro damage evolution of ternary polypropylene blend with ethylene-propylene-rubber (EPR) and talc*", Journal of Solid Mechanics and Materials Engineering, 2 (8), 1018-1036, (2008)

Martin J., Ph.D. Thesis, UPVM-Supélec, Metz, France (2009)

Martin, J., Ponçot, M., Bourson, P., Dahoun, A., Hiver, J.M., "*Study of the Crystalline Phase Orientation in Uniaxially Stretched Polypropylene by Raman Spectroscopy: Validation and Use of a Time-Resolved Measurement Method*", Polymer Engineering and Science, 51 (8), 1607-1616, (2011)

Martin J., Ponçot M., Hiver J.M., Bourson P., Dahoun A., "*Real-time Raman spectroscopy measurements to study the uniaxial tension of iPP: a global overview of microstructural deformation mechanisms*", Journal of Raman Spectroscopy, 44, 776-784, (2013)

Naqui S.I., Robinson I.M., "*Review tensile dilatometric studies of deformation in polymeric materials and their composites*", Journal of Materials Science, 28, 1421-1429, (1993)

Natta G., Corradini P., "*Structure and properties of isotactic polypropylene*", Il Nuovo Cimento, 15 (1), 40-51, (1960)

Natta G., Peraldo M., Corradini P., "*Smectic mesomorphic form of isotactic polypropylene*", Rendiconti Accademia Nazionale Lincei, 26, 14-17, (1959)

Nitta K.H., Yamaguchi M., "*Morphology and mechanical properties in blends of polypropylene and polyolefin-based copolymers*", Polyolefin Blends, Domasius Nwabunma and Thein Kyu-Willey, 224-268, (2008)

Pawlak A., Galeski A, Rozanski A, "*Cavitation during deformation of semicrystalline polymers*", Progress in Polymer Science, 39 (5), 21-958, (2014)

Peterlin A., "*Molecular model of drawing polyethylene and polypropylene*", Journal of Materials Science, 6, 490-508, (1971)

Plummer C.J. Jr., Kausch H.H., "*Deformation and entanglement in semi-crystalline polymers*", Journal of Macromolecular Science – Physics, B35 (3, 4), 637-657, (1996)

Ponçot M., Ph.D. Thesis, INPL-ENSMN, Nancy, France (2009)

Ponçot M., Martin J., Dahoun A., Hiver J.M., Bourson P., Verchère D., "*Shrinkage Study of Polypropylene Films Laminated on Steel-Influence of the Conformation Processes*", American Institute of Physics Conference Proceeding, 1353, 744–749, (2011)

Ponçot M., Martin J., Hiver J.M., Verchère D., Dahoun A., "*Study of the dimensional instabilities of laminated polypropylene films during heating treatments"*, Journal of Applied Polymer Science, 125 (5), 3385-3395, (2012)

Ponçot M., Addiego F., Dahoun A., "*True intrinsic mechanical behavior of semi-crystalline and amorphous polymers: Influences of volume deformation and cavities shape*", International Journal of Plasticity, 40, 126-139, (2013)

Pukanszky B., Van Es M., Mauer F.H.J., Voros G., "*Micromechanical deformations in particulate filled thermoplastics: volume strain measurements*", Journal of Materials Science, 29 (9), 2350-2358, (1994)

Purvis J., Bower D.I., "*Molecular orientation in poly(ethylene terephthalate) by means of laser–Raman spectroscopy*", Journal of Polymer Science: Polymer Physics Edition, 14, 1461-1484, (1976)

Samuels R.J., *Plastic Deformation of Polymers*, Ed. Peterlin A., Marcel Dekker Inc., New York, (1971)

Séguela R., "*On the natural draw ratio of semi-crystalline polymers: review of the mechanical, physical and molecular aspects*", Macromolecular Material Engineering, 292, 235-244, (2007)

Schultz J., *Polymer Materials Science*, Ed. Printice-Hall, Englewood Cliffs, (1974)

Steenbrink A.C., Van der Giessen E., Wu P.D., "*Void growth in glassy polymers*", Journal of the Mechanics and Physics of Solids, 45 (3), 405-437, (1997)

Tadokoro H., Kobayashi M., Ukita M., Yasufuku K., Murahashi S., Torii T., "*Normal vibrations of the polymer molecules of helical conformation: V. Isotactic polypropylene and its deuteroderivatives*", Journal of Chemical Physics, 42(4), 1432-1448, (1965)

Tanaka M., Young R.J., "*Review Polarised Raman spectroscopy for the study of molecular orientation distributions in polymers*", Journal of Materials Science, 41, 963-991, (2006)

Turner-Jones A., Cobbold A. J., "*The β crystalline form of isotactic polypropylene*", Journal of Polymer Science, Part B: Polymer Letters, 6 (8), 539-546, (1968)

van der Wal A., Gaymans R.J., "*Polypropylene-rubber blends: 5. Deformation mechanism during fracture*", Polymer, 40, 6067-6075, (1999)

Ward I.M., *Mechanical Properties of Solid Polymers*, Wiley-Interscience, London, (1971)

Wu S., "*Phase structure and adhesion in polymer blends: a criterion for rubber toughening*", Polymer, 26, 1855-1863, (1985)

Ye J., Ph.D. Thesis, Lorraine University-LEMTA-ENSEM, Nancy, France (2015)

Zebarjad S.M., Bagheri R., Lazzeri A., Serajzadeh S., "*Dilatational shear bands in rubber modified isotactic polypropylene*", Materials and Design, 25, 247-250, (2004)

Figures captions:

Figure 1: 1) Tensile test machine, 2) Dumbbell-shape specimen, 3) Z-motorized stage, 4) Video camera, 5) Raman head of probe, 6) VidéoTraction™ camera, 7) X-rays monochromator.

Figure 2: a) True mechanical behaviors and b) volume strain curves as a function of true strain of iPP, iPP/EPR and iPP/EPR + 7%wt. µ-talc at ambient temperature and constant true strain rate of 5.10^{-3} s^{-1}.

Figure 3: True mechanical behaviors of a) iPP, b) iPP/EPR and c) iPP/EPR + 7 %wt. µ-talc as a function of strain rates at the ambient temperature.

Figure 4: *In situ* evolutions of the 2D WAXS patterns of a) iPP, b) iPP/EPR and c) iPP/EPR + 7 %wt. µ-talc stretched at 22 °C and 5.10^{-4} s^{-1} and recorded at different true strain levels. The stretching direction (I) is vertical.

Figure 5: *In situ* evolutions of the Hermans' factor $F_{(040)/I}$ as a function of the axial true strain of a) iPP, b) iPP/EPR and c) iPP/EPR + 7 %wt. µ-talc stretched at 22 °C.

Figure 6: *In situ* evolutions of the crystalline chains orientation determined by Raman spectroscopy at the ambient temperature as a function of the true strain rates in case of a) iPP, b) iPP/EPR and c) iPP/EPR + 7 %wt. µ-talc.

Figure 7: Correlations between the evolutions of the normalized orientation factors determined by Raman spectroscopy and 2D WAXS at the ambient temperature as a function of the true strain rates in case of a) iPP, b) iPP/EPR and c) iPP/EPR + 7 %wt. µ-talc.

Figure 8: a) α monoclinc crystals of iPP (Cylinders represent the macromolecules), b) macromolecule segment of the helical helix of iPP (Natta and Corradini, 1960).

Figure 9: Equatorial WAXS diffractograms evolution of a) iPP and b) iPP/EPR as a function of stretching.

Figure 10: Comparison of the true intrinsic mechanical behaviors of iPP, iPP/EPR and iPP/EPR + 7%wt. µ-talc at ambient temperature and constant true strain rate of 5.10^{-3} s^{-1} (Ponçot *et al.*, 2013).

Figure 11: Representation of the dilatational shear bands which is developed during uniaxial stretching of iPP/EPR blend (Ponçot, 2009). The tensile direction (I) is vertical.

Figure 12: Scanning electron microscopy images of iPP/EPR and iPP/EPR + µ-talc uniaxially stretched at the ambient temperature and 5.10^{-4} s^{-1} (Ponçot, 2009). Short dashed circle schematizes the circular cross section of the Raman laser and the solid square the beam cross section of X-rays. The tensile direction (I) is vertical.

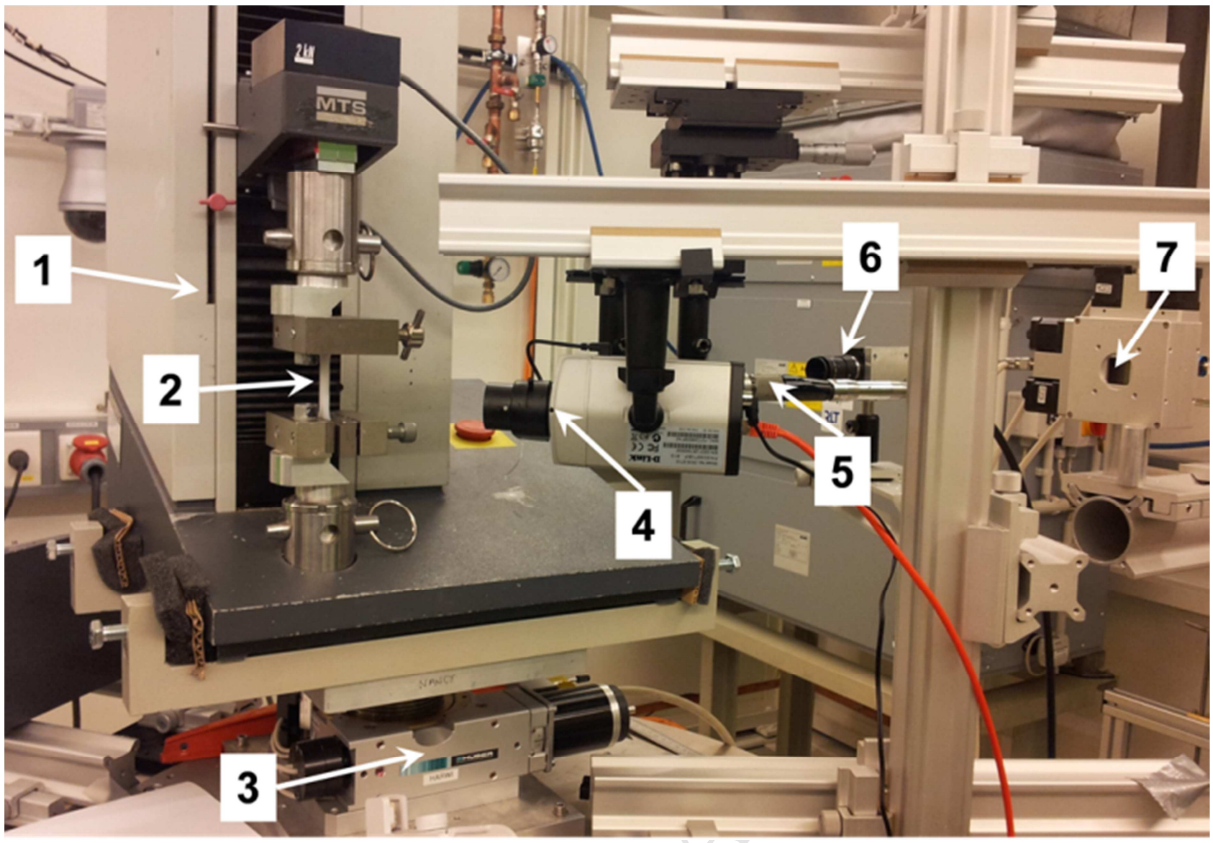

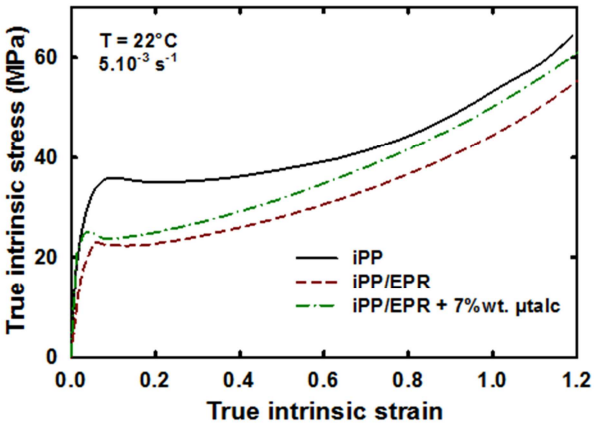

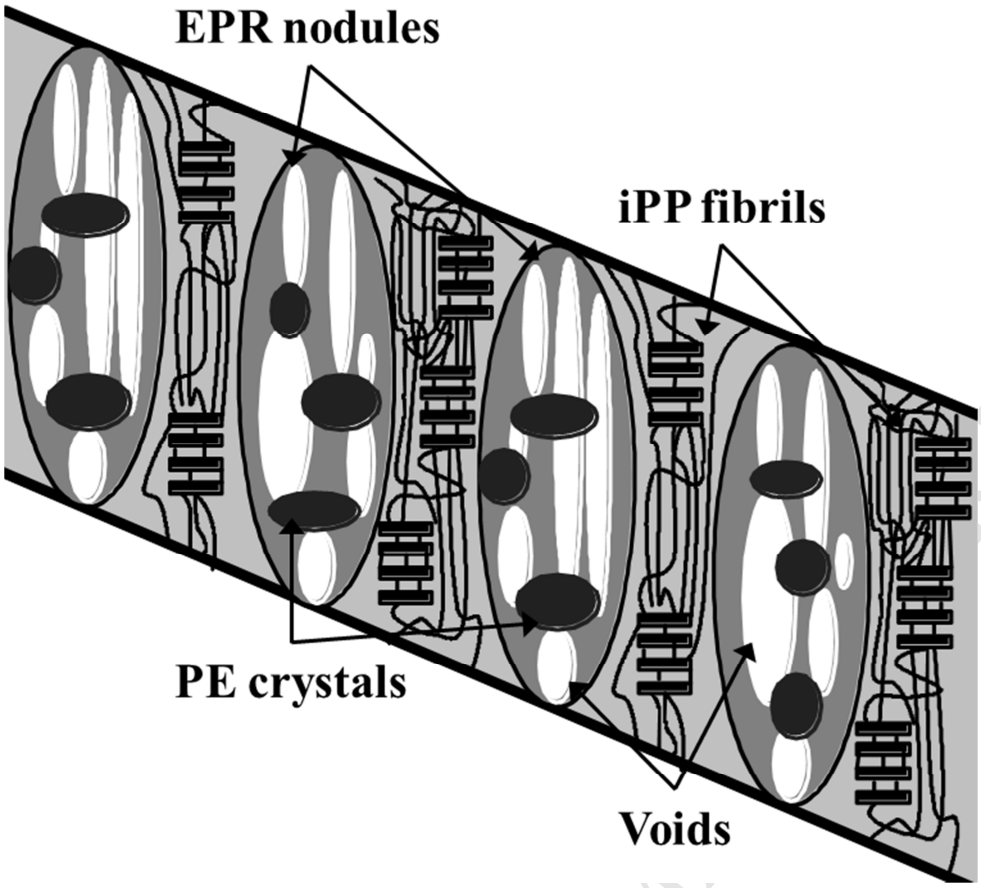

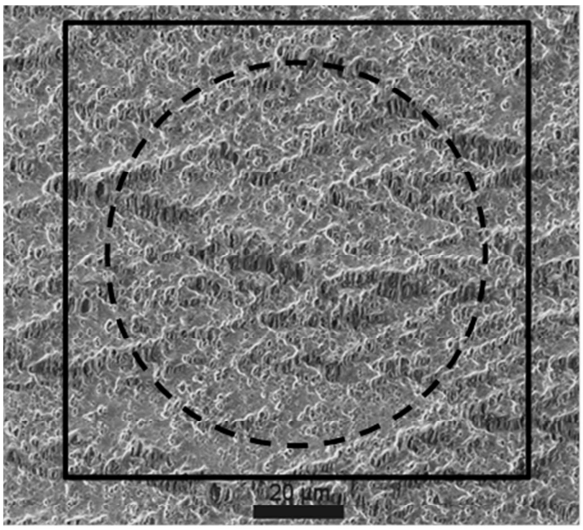

iPP/EPR ➔ $\varepsilon = 0.8$ ($\varepsilon_v = 0.32$)

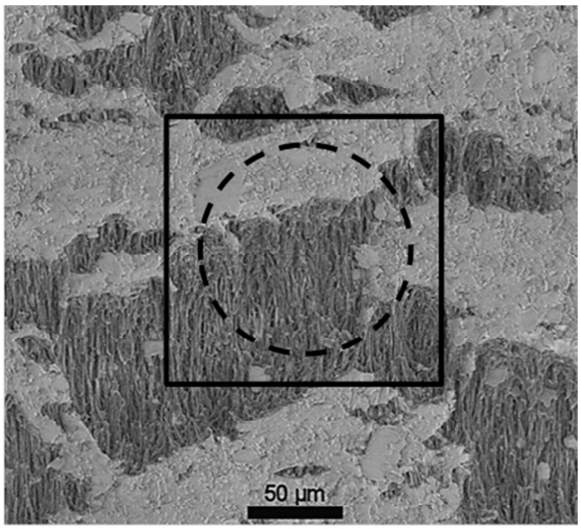

iPP/EPR + µ-talc ➔ $\varepsilon = 0.7$ ($\varepsilon_v = 0.56$)

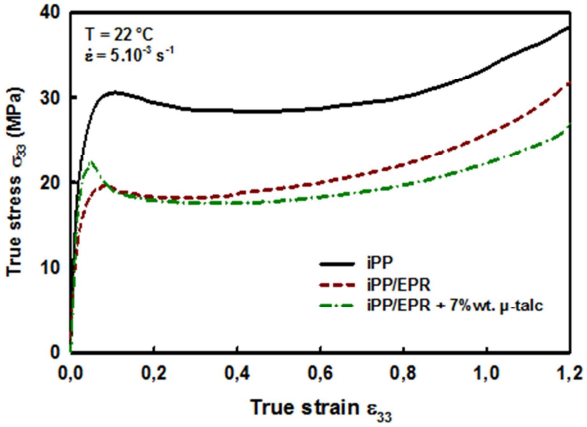

a)

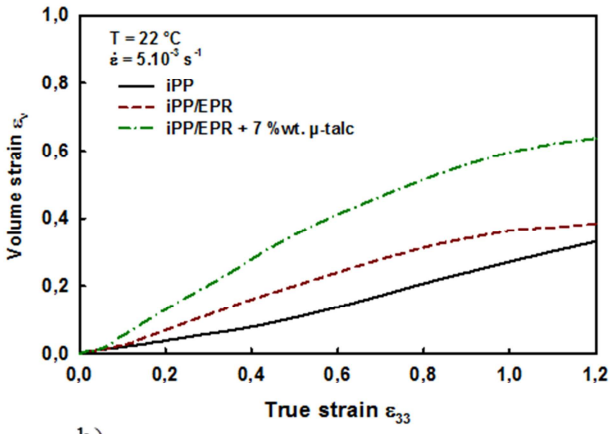

b)

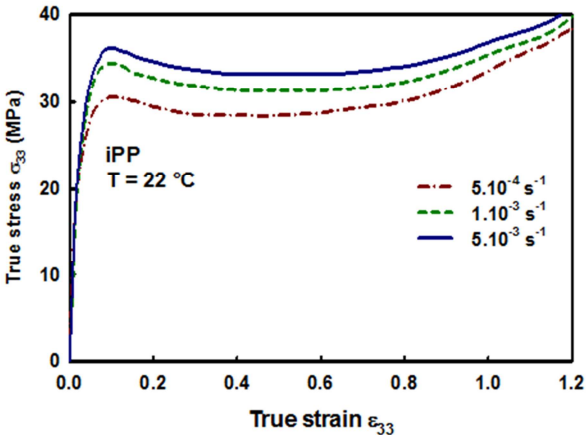

a)

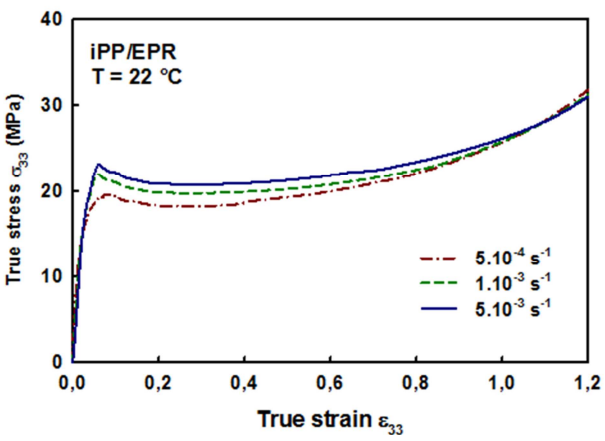

b)

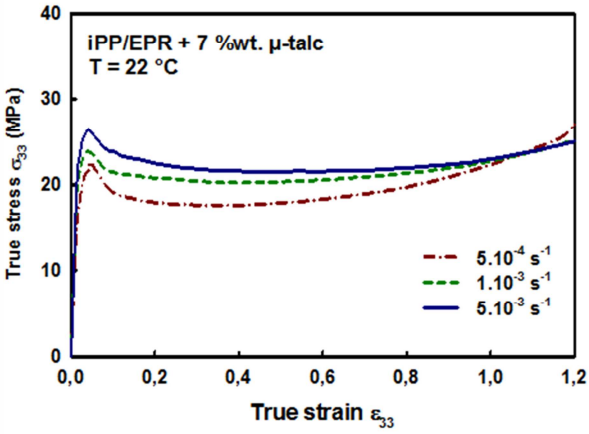

c)

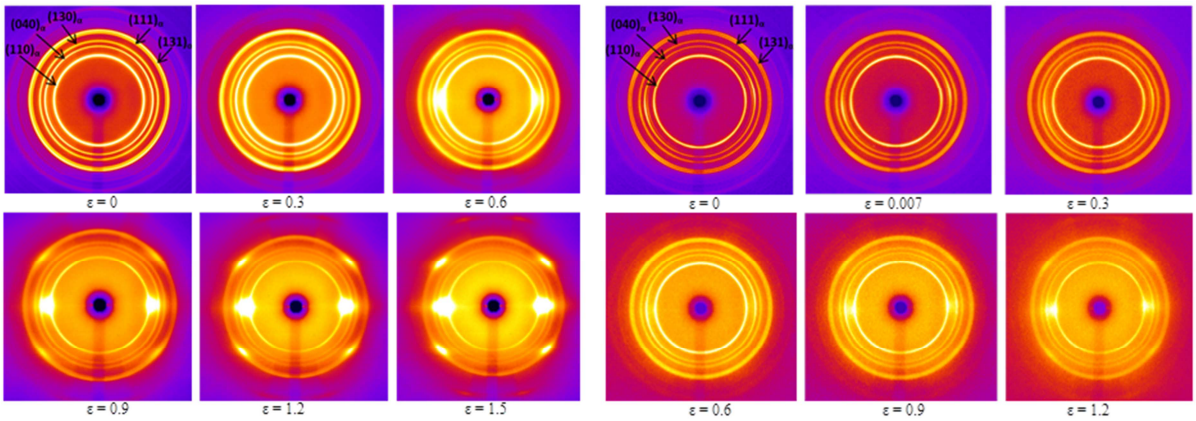

a)

b)

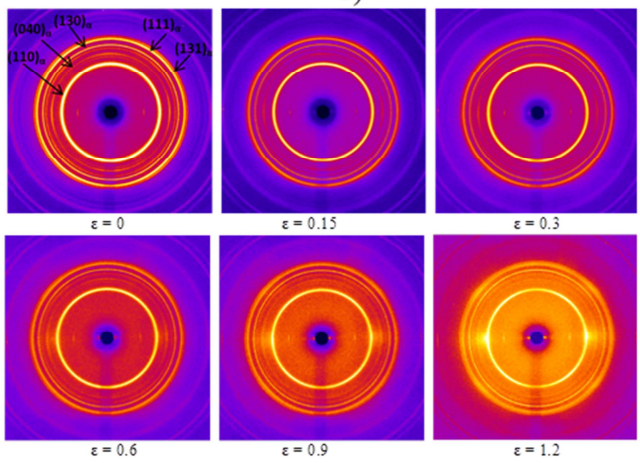

c)

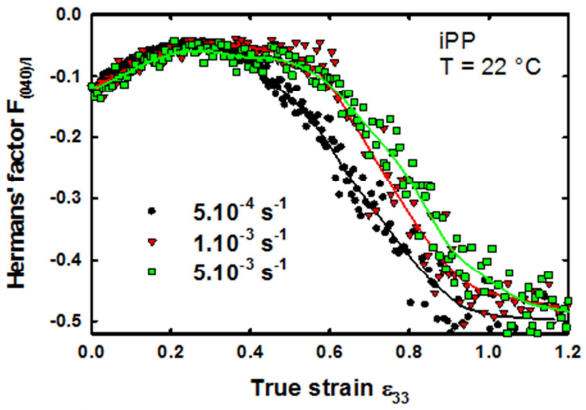

a)

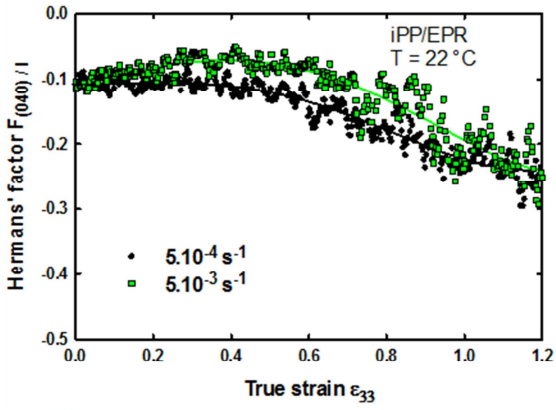

b)

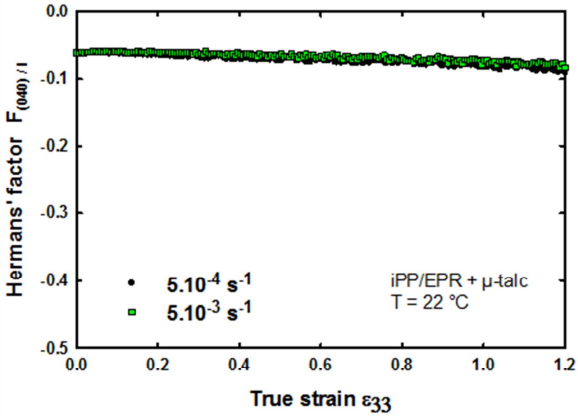

c)

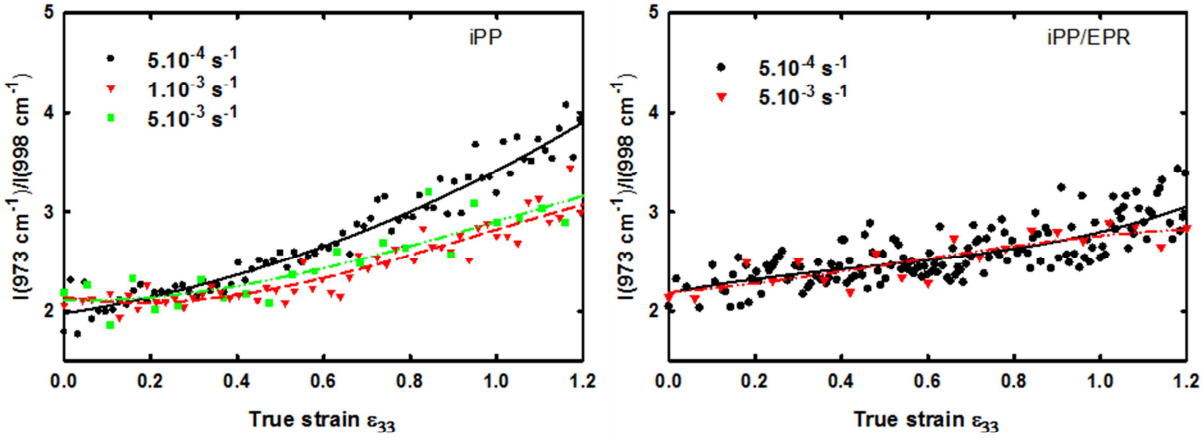

a) b)

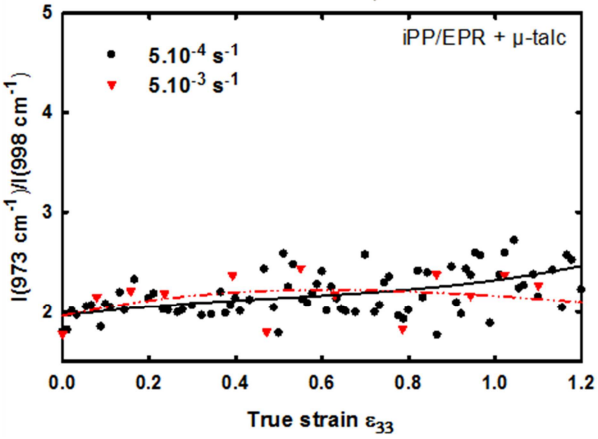

c)

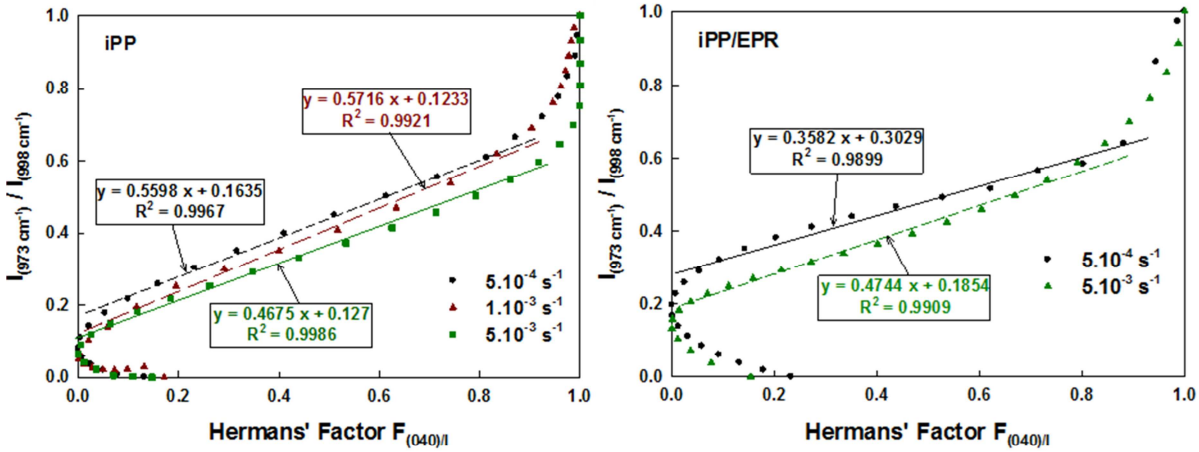
iPP
y = 0.5716 x + 0.1233
R2 = 0.9921
y = 0.5598 x + 0.1635
R2 = 0.9967
y = 0.4675 x + 0.127
R2 = 0.9986
5.10-4 s-1
1.10-3 s-1
5.10-3 s-1
I(973 cm-1) / I(998 cm-1)
Hermans' Factor F(040)/I
a)
iPP/EPR
y = 0.3582 x + 0.3029
R2 = 0.9899
y = 0.4744 x + 0.1854
R2 = 0.9909
5.10-4 s-1
5.10-3 s-1
I(973 cm-1) / I(998 cm-1)
Hermans' Factor F(040)/I
b)

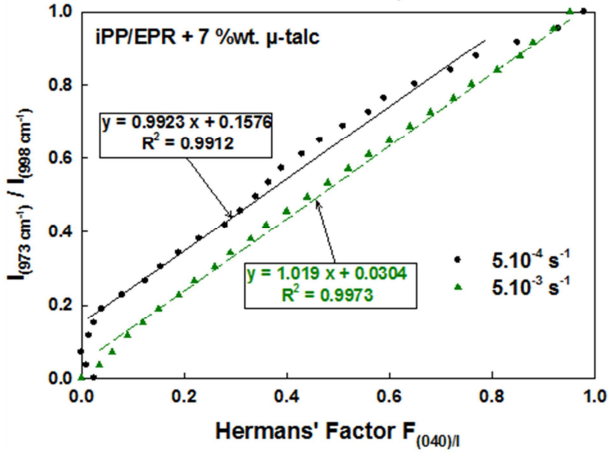
iPP/EPR + 7 %wt. µ-talc
y = 0.9923 x + 0.1576
R2 = 0.9912
y = 1.019 x + 0.0304
R2 = 0.9973
5.10-4 s-1
5.10-3 s-1
I(973 cm-1) / I(998 cm-1)
Hermans' Factor F(040)/I
c)

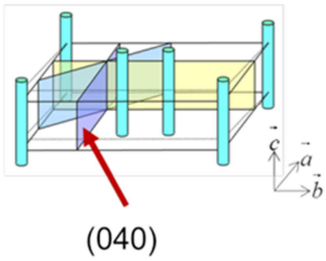

a)

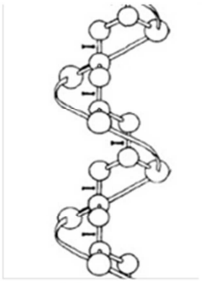

b)

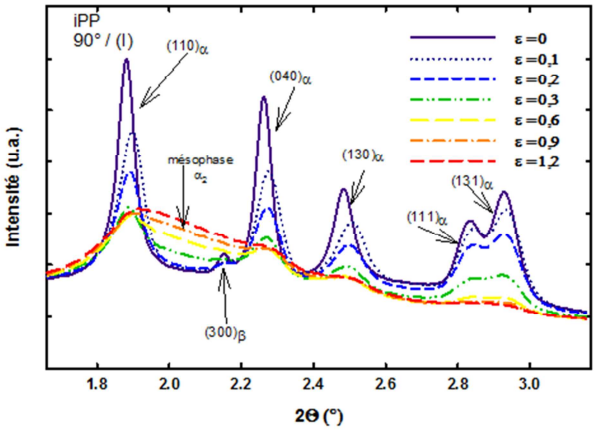

a)

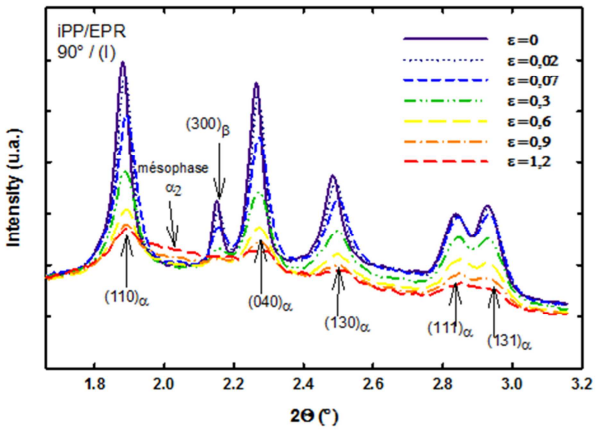

b)

Highlights:

- We study the micromechanisms of deformation involved during uniaxial stretching of three different iPP blends (neat isotactic polypropylene, high impact polypropylene, and high impact polypropylene filled by 7%wt of µ-talc particles) at various strain rates (5.10^{-3} s^{-1}, 10^{-3} s^{-1} and 5.10^{-4} s^{-1}).
- A special experimental set up was developed to perform simultaneous high energy wide angle X-rays scattering (P07 beamline, PETRA III, DESY synchrotron, Hamburg, Deutschland) and Raman spectroscopy analysis during the mechanical test.
- Complementarities and singularities of both techniques to characterize the polymer microstructure are put in evidence.
- Taking into account the *in situ* measured volume strain, the true intrinsic mechanical behaviors of blends are obtained and similar stress hardening slopes are observed which means that a similar fibrillar microstructure is reached.
- Both techniques are not able to measure this high orientation level located in fibrils in case of filled iPP due to their two large volume of analysis (the volume fraction of oriented fibrils is too small in comparison of voids volume fraction, fillers volume fraction and undamaged iPP matrix fraction).